Monte Carlo Simulation of Impurity Scattering Effect in Resonant-Phonon-Assisted Terahertz Quantum-Cascade Lasers *

Cao Juncheng† and L üWingtao

(State Key Laboratory of Functional Materials for Informatics, Shanghai Institute of Microsystem and Information Technology, Chinese Academy of Sciences, Shanghai 200050, China)

Abstract: We study the influence of ionized impurity scattering on the electron transport in resonant-phonon-assisted terahertz (THz) quantum-cascade lasers (QCLs). We treat the ionized impurity scattering rates within the single subband static screening approximation. We find that the ionized impurity scattering supplies an additional current channel across the device, and affects the electrondistribution in different subbands. We conclude that the ionized impurity scattering should be taken into account in the study of the transport properties of resonant-phonon-assisted THz QCLs.

Key words: THz; quantum-cascade laser; Monte Carlo method
EEACC: 0240G
CLC number: TN302 **Document code:** A **Article ID:** 0253-4177(2006)02-0304-05

1 Introduction

Recent developments in the design and fabrication of compact solid state terahertz (THz) sources[1~4] and detectors[5] have opened a bright future for applications of THz technology[6~11]. The development of THz quantum-cascade lasers (QCL) in the past several years makes it one of the most important sources in the THz range. THz QCLs based on different design approaches for carrier extraction have been realized, among which are interminiband transitions[1], resonant-phonon-assisted intersubband transitions[2,4], and bound to continuum transitions[3]. The resonant-phonon-assisted THz QCLs show better temperature performance than other designs[12]. Different theoretical models have been used in the design and simulation of THz QCLs[13~19]. Among them, the Monte Carlo (MC) method[13~16,18] is thought to be the most suitable. The commonly used rate equation method in the design of mid-infrared QCLs cannot take fully into account the complexity of temperature and density dependent scattering times in THz QCLs. And the quantum mechanics approaches are all nontrivial[18,19]. Using the MC method, we can intentionally turn on and off each mechanism to study its influence on the transport properties of the device. In this paper, we study the influence of the ionized impurity scattering on the transport properties of resonant-phonon-assisted THz QCLs.

2 Monte Carlo model

Our MC model follows a conventional scheme of an ensemble of particles[20]. Electron-LO-phonon, electron-electron (e-e) and electron-ionized-impurity (e-imp) scatterings are taken into account. The hot phonon effect is incorporated into the MC procedure within the relaxation time approximation[21]. The electron eigenstates and energy band profile are obtained by solving the effective mass Schrödinger equation for a band structure spanning three modules.

Due to the low Al composition in the simulated structure, the bulk LO phonon scattering is a good approximation[15]. We do not take into ac-

* Project supported by the National Fund for Distinguished Young Scholars of China (No. 60425415), the Major Project of the National Natural Science Foundation of China (No. 10390162), and the Shanghai Municipal Commission of Science and Technology (No. 03JC14082)

† Corresponding author. Email: jccao@mail.sim.ac.cn

Received 26 October 2005

count the phonon confinement effect here[22,23]. The electron-LO-phonon scattering rate under this approximation can be written as

$$\Gamma_{ij}(k) = \frac{m^* e^2 \omega_0}{2\hbar^2}\left(\frac{1}{\varepsilon_\infty} - \frac{1}{\varepsilon}\right) \times \left(N_q \int_0^{2\pi} d\theta \frac{H_{ij}(q_+)}{(q_+^2 + q_s^2)^{1/2}} + (N_q + 1)\int_0^{2\pi} d\theta \frac{H_{ij}(q_-)}{(q_-^2 + q_s^2)^{1/2}} \right) \quad (1)$$

where H_{ij} is given by

$$\frac{H_{ij}(q)}{(q^2 + q_s^2)^{1/2}} = \int_{-\infty}^{\infty} dz \int_{-\infty}^{\infty} dz' \rho_{ij}(z) \rho_{ij}^*(z') I(q, z, z') \quad (2)$$

$$I(q, z, z') = \frac{\exp[-(q^2 + q_s^2)^{1/2} | z - z' |]}{(q^2 + q_s^2)^{1/2}} \times \left(1 - \frac{| z - z' | q_s^2}{2(q^2 + q_s^2)^{1/2}} - \frac{q_s^2}{2(q^2 + q_s^2)}\right) \quad (3)$$

and

$$q = | k - k' | = \left[2k^2 \pm \frac{2\omega_{ij}^* m^*}{\hbar} - 2k\left(k^2 \pm \frac{2\omega_{ij}^* m^*}{\hbar} \right)^{1/2} \cos\theta \right]^{1/2} \quad (4)$$

$$\hbar\omega_{ij}^* = \hbar\omega_0 \pm (E_i - E_j) \quad (5)$$

Here, e is the elementary charge, m^* is the electron effective mass, $\hbar$ is the reduced Planck constant, and ε_∞ and ε are the high frequency and low frequency dielectric constants, respectively. N_q is the LO phonon occupation number. $\rho_{ij}(z) = \zeta_i^*(z)\zeta_j(z)$, $\zeta_i(z)$ and $\zeta_j(z)$ are the electron envelope functions for the ith and jth subbands, respectively. k and k′ are the electron wave vectors before and after scattering, respectively. The + and - signs on q refer to the absorption and emission of LO phonons, respectively. q_s is the inverse screening length, which is taken to be zero.

For the e-e scattering, we use the single subband static screening model, and only take into account interactions between electrons in the same or neighbour modules. All the simulated electrons are assumed to be in one module. Those that are scattered out of the module are re-injected into the corresponding subband according to the periodic boundary conditions. The scattering rates for an electron in subband i with wave vector k to subband j with wave vector k′ can be written as[24,25]

$$\Gamma_{ij}(k) = \frac{e^4 m^*}{16\pi\hbar^3 \varepsilon^2 \varepsilon_0 A} \sum_{k_0, m, n} f_m(k_0) \int_0^{2\pi} d\theta \frac{| F_{imjn}(q) |^2}{(q + q_s)^2} \quad (6)$$

where

$$F_{imjn}(q) = \int_z \int_{z'} \zeta_n^*(z') \zeta_j^*(z) \zeta_i(z) \zeta_m(z') \times \exp(-q | z - z' |) \quad (7)$$

$$(2q)^2 = 2g^2 + \Delta k_0^2 - 2g\sqrt{g^2 + \Delta k_0^2}\cos\theta \quad (8)$$

$$\Delta k_0^2 = \frac{4m^*}{\hbar^2}(E_i + E_m - F_j - E_n) \quad (9)$$

$$g^2 = k^2 + k_0^2 - 2kk_0\cos\alpha$$

The e-e scattering is a dual-particle process. During the process, another electron initially in subband m with wave vector k_0 is scattered to subband n with wave vector k′. The quasi-2D inverse screening length q_s in the single subband static screening approximation is

$$q_s = \frac{m^* q^2}{2\pi\varepsilon_0 \varepsilon \hbar^2} n_1, \quad k = 0 \quad (11)$$

The e-e scattering rates are included in the MC procedure by using the method of Goodnick et al.[24]

Similar to e-e scattering, the e-imp scattering is also taken into account by using the single subband static screening approximation. The scattering rate from subband i to subband j is given by[26,27]

$$\Gamma_{ij}(k) = \frac{m^* e^4}{8\pi\hbar^3 \varepsilon_0^2 \varepsilon^2} \int_0^{2\pi} d\theta (1 - \cos\theta) \times \left(\frac{1}{q\varepsilon(q)}\right)^2 \int_z | E_{ij}(q, z) |^2 n(z) \quad (12)$$

where $q = 2k\sin(\theta/2)$, n(z) is the doping density, the form factor F_{ij} reads

$$F_{ij}(q, z) \int_{z'} \zeta_j^*(z') \zeta_i(z') \exp(-q | z - z' |) \quad (13)$$

and

$$q\varepsilon(q) = \begin{cases} q + CG(q), & q \le 2k_F \\ q + C(1 - [1 - (2k_F/q)^2]^{1/2})\, G(q), & q > 2k_F \end{cases} \quad (14)$$

where k_F is the Fermi wave vector, $C = m^* e^2 / 2\pi\hbar^2\varepsilon_0\varepsilon$, and

$$G(q) = \int_z \int_{z'} \zeta_i(z) \zeta_j^*(z) \zeta_i(z') \zeta_j^*(z') \times \exp(-q | z - z' |) \quad (15)$$

The hot phonon dynamics can be incorporated into the MC procedure by following the method of Lugli et al.[21]. The time evolution of the LO phonon population is followed, and its modification to the electron-phonon interaction is considered. The LO phonon decay into other modes is taken into account by introducing the relaxation time τ_{ph}. In detail, the perpendicular component q_z is tabulated for discrete values corresponding

to intra- and inter-subband transitions, respectively. It is zero for intrasubband transitions, and is a non-zero value related to the subband energy difference for intersubband transitions. The in-plane component of the phonon wave vector $q_{\parallel}$ is treated as two-dimensional, and is discretized into small cells. The phonon number in each cell is initialized as the Bose distribution. After each LO phonon emission/absorption, their values are updated in the corresponding cell as

$$\delta N_q = \pm \frac{2\pi}{\delta q_x} \times \frac{2\pi}{\delta q_y} \times \frac{n_s}{N} \tag{16}$$

Here δq_x and δq_y are the cell size in the x and y directions, respectively, n_s is the electron sheet density, and N is the number of particles included in the MC simulation. At the end of each time interval, the phonon number is recalculated as

$$N'_q(i\delta t) = N_q(i\delta t) - [N_q(i\delta t) - N_q(0)]\frac{\delta t}{\tau_{ph}} \tag{17}$$

where δt is the time interval in the MC simulation, which is chosen to be much smaller than τ_{ph}.

3 Effect of ionized impurity scattering

The structure parameters of the simulated device are based on a recent lasing THz QCL[4]. The active region of the THz QCL is based on a 4-well module design in which the THz generating transition is from a pair of anti-crossed double-well states, a wide and doped subsequent well provides the LO phonon mediated relaxation, and the injection to the following double well is from an undoped well. Beginning with the first injection barrier, the layer thicknesses of the 4-well module are 5.4/7.8/2.4/6.4/3.8/15.3/3.5/8.8 in nm, where the barrier layers are shown in bold and the doped layer is underlined. A schematic of the conduction band structure under an electric field of 12 kV/cm is shown in Fig. 1, together with the squared wave functions of the most important states. The doping density is $3.2 \times 10^{10}\,cm^{-2}$, the lattice temperature is taken to be 25 K, and the decay time of polar optical phonons is 5ps.

The e-imp scattering is similar to the e-e scattering. They are both coulombic interactions. they should also play similar roles in the transport properties of QCLs. As we know, the e-e scattering is important in coupling the near resonant states between the active region and the injector/collector region, while the electron-LO-phonon scattering is important for electronic cascade within the active region. The e-imp scattering provides an additional channel connecting the injector/collector region and the active region. Our simulation results support these qualitative judgments. In Fig. 2, we show the time derivation of the subband occupation with and without the e-imp scattering. For each case, the curves from high to low concentration correspond to subbands 2, 1, 5, 3, 4, respectively. We can see that in the presence of the e-imp scattering, electrons redistribute among three subbands 1, 2, and 5. The electron concentration in subband 5 increases greatly, and the corresponding population inversion is also enhanced. Thus the e-imp scattering is an efficient channel of electron injection/subtraction. Due to the short electron lifetime in subbands 3 and 4, their concentrations are little affected by the e-imp scattering. Our simulation results also show that the electron current across the device increases due to this additional current channel. It changes from 900 to about 1300A/cm^{-2}. The electron current that we get here is larger than the experimental result. This is attributed to the coherent model, which is used to get the electron wave functions here. In real devices, wave function localization due to interface roughness, alloy, and impurity scattering is important. This makes the electron injection and subtraction process much less efficient than predicted by the coherent model. The use of the tight binding model within the density matrix formalism may solve

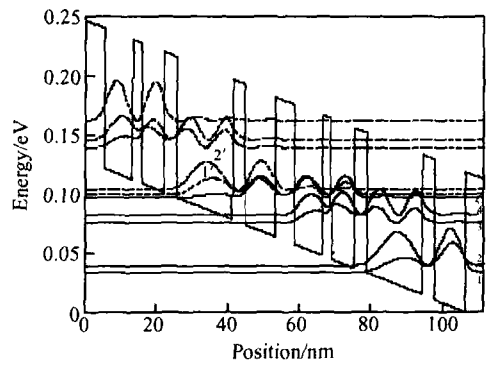

Fig. 1 Schematic conduction band profile and squared wave functions of the THz QCL under an electric field of 12kV/cm The eigen energies and wave functions are obtained by solving the effective mass Schrödinger equation for a band structure spanning three modules. Only two modules are shown here.

this problem[15].

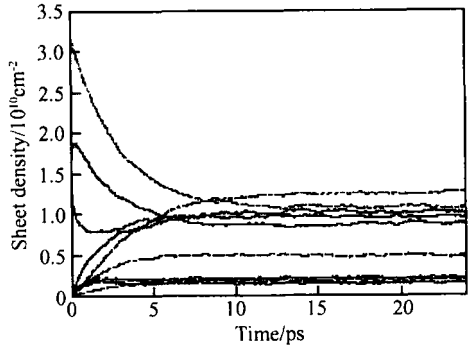

Fig. 2 Time derivation of subband occupation in one module The dashed lines are results without taking into account the electron-ionized-impurity scattering, and the solid lines with this effect. For both cases, from high to low concentration the five lines correspond to subband indices 2,1,5,3,4, respectively.

4 Conclusion

In summary, we have studied the influence of the ionized impurity scattering on transport properties of resonant-phonon-assisted THz QCLs by using the Monte Carlo method. This scattering mechanism is as important as the e-e scattering in the electron injection and subtraction process. The electrons redistribute in different subbands, and the device current increases due to the presence of e-imp scattering. Thus we have to include it in the simulation of THz QCLs. The overestimation of the current when including the e-imp scattering is due to the exclusion of wave function localization in the present model.

References

[1] Köhler R, Tredicucci A, Beltram F, et al. Terahertz semiconductor heterostructure laser. Nature, 2002, 417: 156

[2] Williams B S, Callebaut H, Kumar S, et al. 3.4-THz quantum cascade laser based on longitudinal-optical-phonon scattering for depopulation. Appl Phys Lett, 2003, 82(7): 1015

[3] Scalari G, Ajili L, Faist J, et al. Far-infrared (λ= 87mm) bound-to-continuum quantum-cascade lasers operating up to 90K. Appl Phys Lett, 2003, 82(19): 3165

[4] Liu H C, Wächter M, Ban D, et al. Effect of doping concentration on the performance of terahertz quantum-cascade lasers. Appl Phys Lett, 2005, 87(14): 141102

[5] Liu H C, Song C Y, Spring Thorpe A J, et al. Terahertz quantum-well photodetector. Appl Phys Lett, 2004, 84(20): 4068

[6] Cao J C. Interband impact ionization and nonlinear absorption of terahertz radiations in semiconductor heterostructures. Phys Rev Lett, 2003, 91: 237401

[7] Cao J C, Liu H C, Lei X L. Simulation of negative-effective-mass terahertz oscillators. J Appl Phys, 2000, 87: 2867

[8] Cao J C, Lei X L. Multiphoton-assisted absorption of terahertz radiations in InAs/AlSb heterojunctions. Phys Rev B, 2003, 67: 085309

[9] Liu H C, Song C Y, Wasilewski Z R, et al. Coupled electron-phonon modes in optically pumped resonant intersubband lasers. Phys Rev Lett, 2003, 90(7): 077402

[10] Cao J C, Lei X L, Li A Z, et al. Spectrum dynamics of negative-effective-mass oscillators under terahertz radiation. Appl Phys Lett, 2001, 78: 2524

[11] L ü T, Cao J C. Terahertz generation and chaotic dynamics in GaN NDR diode. Semicond Sci Technol, 2004, 19: 451

[12] Williams B S, Kumar S, Callebaut H, et al. Terahertz quantum-cascade laser operating up to 137K. Appl Phys Lett, 2003, 83(25): 5142

[13] Iotti R C, Rossi F. Microscopic theory of hot-carrier relaxation in semiconductor-based quantum-cascade lasers. Appl Phys Lett, 2000, 76(16): 2265

[14] Kohler R, Iotti R C, Tredicucci A, et al. Design and simulation of terahertz quantum cascade lasers. Appl Phys Lett, 2001, 79(24): 3920

[15] Callebaut H, Kumar S, Williams B S, et al. Analysis of transport properties of terahertz quantum cascade lasers. Appl Phys Lett, 2003, 83(2): 207

[16] Indjin D, Harrison P, Kelsall R W, et al. Self-consistent scattering model of carrier dynamics in GaAs-AlGaAs terahertz quantum-cascade lasers. IEEE Photonics Technol Lett, 2003, 15: 15

[17] Iotti R C, Rossi F. Nature of charge transport in quantum-cascade lasers. Phys Rev Lett, 2001, 87(14): 146603

[18] Lee S C, Wacker A. Nonequilibrium green's function theory for transport and gain properties of quantum cascade structures. Phys Rev B, 2002, 66(24): 245314

[19] Callebaut H, Kumar S, Williams B S, et al. Importance of electron-impurity scattering for electron transport in terahertz quantum-cascade lasers. Appl Phys Lett, 2004, 84(5): 645

[20] Jacoboni C, Lugli P. The Monte Carlo method for semiconductor device simulation. New York: Springer-Verlag Wien, 1989

[21] Lugli P, Jacoboni C, Reggiani L, et al. Monte Carlo algorithm for hot phonons in polar semiconductors. Appl Phys Lett, 1987, 50(18): 1251

[22] L ü T, Cao J C. Interface and confined optical-phonon modes in wurtzite multi-interface heterostructures. J Appl Phys, 2005, 97(3): 033502

[23] L ü T, Cao J C. Confined optical phonon modes and electron-phonon interactions in wurtzite GaN/ZnO quantum wells. Phys Rev B, 2005, 71(15): 155304

[24] Goodnick S M, Lugli P. Effect of electron-electron scattering on nonequilibrium transport in quantum-well systems. Phys Rev B, 1988, 37(5): 2578

[25] Mosko M, Moskovà A, Cambel V. Carrier-carrier scattering in photoexcited intrinsic GaAs quantum wells and its effect on femtosecond plasma thermalization. Phys Rev B, 1995, 51(23): 16860

[26] Ando T, Fowler A B, Stern F. Electronic properties of two

- dimensional systems. Rev Mod Phys, 1982, 54(2): 437
[27] Watling J R, Walker A B, Harris J J, et al. Monte Carlo simulation of electron transport in highly delta - doped GaAs/ AlGaAs quantum wells. Semicond Sci Technol, 1998, 13:43

共振声子辅助的太赫兹量子级联激光器中杂质散射的蒙特卡洛模拟 *

曹俊诚† 吕京涛

(中国科学院上海微系统与信息技术研究所 信息功能材料国家重点实验室, 上海 200050)

摘要: 通过蒙特卡洛方法研究了基于共振声子散射的太赫兹量子级联激光器中杂质散射对激光器性能的影响. 使用单子带静态屏蔽模型来处理电子与杂质的散射过程. 发现电子与杂质的散射为电子在有源区中的注入和抽取过程提供了另外一个通道. 这一过程可以影响电子在不同子带的占据数以及器件的电流. 所以, 在考虑基于共振声子散射的太赫兹量子级联激光器中的电子输运过程时, 需要包含电子与杂质的散射过程.

关键词: 太赫兹; 量子级联激光器; 蒙特卡洛方法
EEACC: 0240G
中图分类号: TN302 **文献标识码**: A **文章编号**: 0253-4177(2006)02-0304-05

* 国家杰出青年基金(批准号:60425415), 国家自然科学基金(批准号:10390162), 及上海市科委(批准号:03JC14082)资助项目
† 通信作者. Email:jccao@mail.sim.ac.cn
2005-10-26 收到